Numerical Study of the High-Speed Leg of a Wind Tunnel

Sudheer Nayani[1] and William L. Sellers, III[2]
Analytical Services & Materials, Inc., Hampton, VA 23666-1340

Scott E. Brynildsen[3]
Vigyan, Inc., Hampton, VA, 23666-1325

Joel L. Everhart[4]
NASA Langley Research Center, Hampton, VA 23681-0001

The paper describes the numerical study of the high-speed leg of the NASA Langley 14 x 22-ft Low Speed Wind Tunnel. The high-speed leg consists of the Settling Chamber, Contraction, Test Section, and First Diffuser. Results are shown comparing two different exit boundary conditions and two different methods of determining the surface geometry.

Nomenclature

q	=	dynamic pressure, $\frac{1}{2}rv^2$
M	=	Mach number
ρ	=	fluid density
t_w	=	wall shear stress
u,v,w	=	velocity components
u^+	=	dimensionless velocity, $u^+ = u/u_t$
u_t	=	friction velocity, $\sqrt{\frac{t_w}{r}}$
y^+	=	dimensionless wall distance $\frac{yu_t}{u}$
u	=	kinematic viscosity

Abbrev

BC	=	Boundary condition
CAD	=	Computer-aided design
CFD	=	Computational fluid dynamics
GIS	=	Geographic Information Systems
Sta.	=	Tunnel station, ft.

I. Introduction

IN the future, aircraft will be much more integrated to enable reduced fuel burn, noise, and emissions. Computational fluid dynamics (CFD) is already making significant inroads in the design process for these advanced vehicle configurations. Experimental data from wind tunnel facilities are still needed to validate the CFD methods, but also to examine off-cruise conditions, and help project the data to flight Reynolds number conditions. To successfully design these new aircraft, it will require using both CFD and experiment and using the best attributes of both techniques.

---

[1] Senior Scientist, CFD Group, 107 Research Drive, Hampton, VA 23666-1340, AIAA Senior Member
[2] Senior Scientist, CFD Group, 107 Research Drive, Hampton, VA 23666-1340, AIAA Associate Fellow
[3] Research Engineer, GeoLab, 30 Research Drive, Hampton, VA 23666-1325
[4] Chief Engineer, MS 225, Hampton, VA 23681-0001, AIAA Associate Fellow

To validate the CFD methods, the experiments must be completely simulated and that may include modeling the tunnel walls, model support systems, or any other features that may affect the wind tunnel data itself. From the experimental side it means one must truly understand the operations of the wind tunnel, the flow characteristics, and wall corrections. The experimentalist must understand what is needed to provide the proper boundary conditions for the CFD simulations and provide that data in the most accurate way possible

Wind tunnel corrections have been around for a long time and include techniques to account for the constraining effect of the walls on the streamlines in the tunnel, blockage effects from the model and support systems, and buoyancy corrections for any longitudinal or streamwise variations in static pressure in the tunnel. The earlier linear methods began to fail as configurations have advanced to include non-linear lift from vortices, high flow turning from advanced flap systems, or cases where the model has large blockage or moves significantly off the centerline. Newer wall correction methods have been developed that use arrays of wall pressures to help mitigate these effects.

Numerical simulations have treated the case of a model in the wind tunnel test section in a variety of ways. Many simulations are run by modeling the test configuration in a box made from the dimensions of the test section, and treating the tunnel walls as inviscid surfaces. Others have extended the cross section of the test section an arbitrary distance ahead of and behind the model to minimize the effects of the model on the entrance and exit boundaries. In cases where there are significant tunnel effects, the simulations have to be more detailed. Rogers[1] presented the results of a CFD validation experiment of a semi-span high-lift model that was tested in the NASA Ames 12-ft Pressure Wind Tunnel. A comparison of the experimental and CFD results at the higher lift conditions indicated that CFD had to fully simulate the experiment, which included tunnel walls, splitter plates, etc. The simulations were run with viscous walls, and the test section was extended to provide a simple inlet and exit configuration. The conventional tunnel modeling techniques were not sufficient in an unpublished study by the authors of a model in a tunnel with unique contraction characteristics, and a model with a wing span that nearly spanned the walls. The CFD predictions did not come close to capturing the lift characteristics of the configurations after simulating the test section alone, with model and the model support system. When the entire settling chamber, contraction, test section and diffuser were modeled the CFD predictions came very close to matching the experimental results.

The simulations mentioned above are sufficient for validating the CFD methods, but do not provide much information regarding what other things might be affecting the tunnel flow. Experimental data covering the cross section of the test section are rare because they are time consuming and expensive. Typically there are a few discrete points inside the test section measuring such things as velocity, flow angles, boundary layer profiles, or longitudinal pressures on the tunnel walls. It is more rare to find a facility that has made flow surveys through other parts of the tunnel circuit. When CFD and Experiment are used together those gaps in the experimentalist knowledge of the facility can be closed.

There have been attempts to model the high-speed leg of a wind tunnel and these have been performed to provide information regarding something that is occurring in the tunnel flow. Most notable are the work of Olander[2] and Wall[3], where they modeled the high-speed leg of the Volvo Slotted Wall Wind Tunnel. The purpose of the work was to try to identify the cause of an asymmetric pressure distribution on the tunnel walls. They modeled the entire first leg of the Volvo tunnel from the settling chamber to the first diffuser. Extensions were added to the entrance to the settling chamber and exit of the diffuser to create a buffer for the exit boundaries. A lot was learned regarding the flow through the slots and how the boundary layer removal system caused the flow to interact with models in the test section. The cause for the asymmetric pressure distribution could not be identified and it was speculated that the entire circuit would need to be simulated to capture the history of the flow before entering the settling chamber.

This paper describes the effort to simulate the high-speed or 1st leg of the NASA Langley 14 x 22-ft Low Speed Wind Tunnel. This facility was chosen because of the earlier work that was done to calibrate the facility and the flow surveys that were done to identify flow features throughout the entire tunnel circuit. The simulations presented will include two different geometry models for the high-speed leg that consists of the settling chamber, test section, and first diffuser. Two different exit boundary conditions are presented and the process that was used to obtain the proper test conditions in the test section for each boundary condition is defined.

II. 14 x 22-Ft Low-Speed Wind Tunnel

The 14 x 22-ft tunnel, shown in Figure 1, was designed and built in 1969 to provide an improved understanding of the aerodynamics of vertical/short takeoff and landing (V/STOL) configurations. The tunnel is a closed circuit, atmospheric wind tunnel with a maximum speed of 338 ft/sec. The test section is 50 ft long. It can be operated in

either a conventional closed configuration or in an open test section configuration made by raising the ceiling and walls to form and floor-only configuration. A 9-bladed, 40 ft diameter fan coupled to a 12,000 hp electric motor powers the tunnel. Figure 2 shows a schematic of the tunnel circuit and Figure 2(b) shows a sketch of the tunnel stations that are referenced in this paper. Tunnel station 0.0 and 50.0 are the entrance and exit of the test section respectively, and tunnel station 192 is the exit of the first diffuser. Tunnel station 7.87 is where measurements of the wall boundary layers were taken during Test 137 just prior to the 1st AIAA High Lift Workshop[4]. Tunnel station 17.75 is at the center of the 1st turntable in the test section and is where models are typically located in the test section. Gentry[5] et. al. provides a complete description of the tunnel and its flow characteristics.

Figure 1 Aerial view of the 14 x 22-ft Low Speed Wind Tunnel

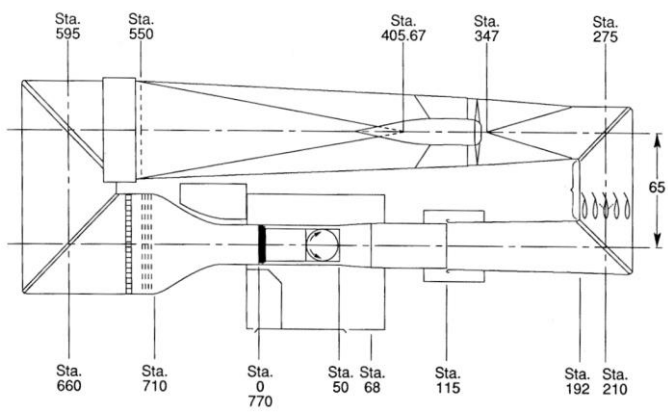

(a) Schematic of the 14 x 22-ft tunnel circuit

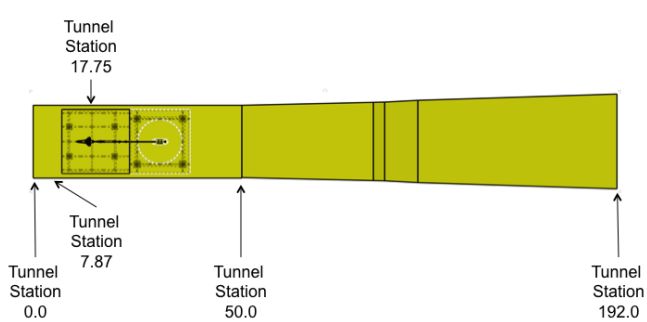

(b) Sketch of tunnel stations

Figure 2 14 x 22-ft Tunnel Layout

A. Geometry Development

Two different methods were used to develop the surface models for the grid generation. The first was based on the original 1965 construction drawings for the facility and the second was based on a laser scanning system that produced what is felt to be the "as-built" geometry. Both methods still required engineering judgment and simplification and that will be described below.

1. Construction Drawings

Construction drawings of the tunnel circuit were used to provide the "as designed" baseline for this study. The geometry data consisted of cross sections through the tunnel circuit. Certain cross-sections that are exposed to the outside elements (e.g. rain) were designed to have a 300-ft radius on the ceiling for water runoff. No information was provided on how the ceiling transitioned from flat to curved, so the cross sections were left as flat. The settling chamber and contraction were simplified and all the details of the honeycomb and screens omitted. The 14 x 22-ft tunnel also has an air exchange vent in the first diffuser that when opened allows fresh air to enter the circuit and is exhausted from the ceiling at the end of the 4th diffuser. The vent was faired over for this study.

2. Laser-scanned Point-cloud

NASA Langley is embarking upon a process to define the geometry of several of the Center's heavily used facilities. The data obtained will serve two purposes; 1) provide a detailed description of the "as built" condition of the facility that can be used to track changes over time, and 2) provide a digital geometric description that can serve to develop computational grids at a later date.

The GIS team at NASA Langley used laser-scanning techniques to provide surface measurements accurate to within a couple of centimeters throughout the 14 x 22-ft tunnel circuit. The point cloud obtained contained approximately 159 million points for the high-speed leg and 587 million points for the entire circuit. The point cloud was transferred to the GeoLab group at Langley to process the point cloud into surfaces to be used for grid generation purposes.

The GeoMagic® software program was used to manually down-sample the point cloud to a particular entity of interest (e.g. test section), and features that were not of interest for this work were excluded (e.g. windows, doors). A best-fit plane/cylinder shape was fit to the points of interest and the deviations from the points were checked to determine if additional points should be added or removed. This process was repeated until a satisfactory fit was obtained. The resulting surface was imported into the Uniqraphics® CAD program to match up the new surface to adjacent features. The Unigraphics surfaces were then imported back into Geomagic software to again check the deviations from the scanned points. This process of matching surfaces in Unigraphics and Geomagic was continually iterated until a suitable surface(s) were obtained. Once the surfaces for the high-speed leg were obtained they were then ready for the grid generation process described below.

The laser-scanned surfaces provide details that were not readily available in the construction drawings. The fairing in the contraction that smooths the flow over the mounting hardware for the honeycomb and screens were identified. The 300 ft radius on the ceiling at several stations in the first diffuser was identified as well as the transitions from the flat to curved ceilings. Most of the deviations between the Construction drawings and scanned surfaces were on the order of a few inches.

III. Numerical Modeling Approach

The computations presented in this paper were obtained using the NASA Tetrahedral Unstructured Software System[6] (TetrUSS) that was developed at the NASA Langley Research Center (LaRC). The system is comprised of several loosely integrated software packages that allow the user to start with a geometry, typically in a CAD or Plot3D format, then generate surface definitions and tetrahedral volume grids for use with the flow solver. The surface definition package (GridTool[7]) allows the user to set up surface patches, boundary conditions, and viscous spacing requirements. The volume grid software package (VGRID) takes the files from GridTool and uses the Advancing Front Method[8] (AFM) to generate the inviscid field cells and the Advancing Layers Method[9] (ALM) to generate thin-layered viscous cells.

B. Flow Solver

The Reynolds averaged Navier-Stokes code, USM3D, described in reference 6 was used for all the calculations presented in this paper. USM3D is a cell-centered, upwind-biased, finite volume flow code that solves the compressible Euler and Navier-Stokes equations on tetrahedral unstructured grids. The computations were performed using 96 processors on the Pleiades Supercomputer at NASA Ames Research Center. Computations were preformed as fully viscous solutions using the Spalart-Allmaras turbulence model for comparison with the wind tunnel data. The Reynolds number for the simulations was 1.71×10^6 per ft, or 116.7×10^6 based on the 99.25 ft run length from the start of the settling chamber to tunnel station 17.75. The target Mach number was 0.2678, which represented a test point of q = 100 lb/ft^2.

C. Grid Generation

The grids were developed using a computational symmetry plane at the centerline. Figure 3 shows a typical surface grid and the typical grid size was approximately 10.7 million cells. The viscous spacing was determined by specifying the Reynolds number and viscous wall spacing $y^+ = 0.5$. Stretching parameters are then specified that blend the viscous grid into the background inviscid grid. A cylindrical source were used in the test section to provide more grid density both on the walls and the field. Additional grids have been developed for examining the Mach number and pressure distributions on the centerline and those grid sizes approached 38 million cells.

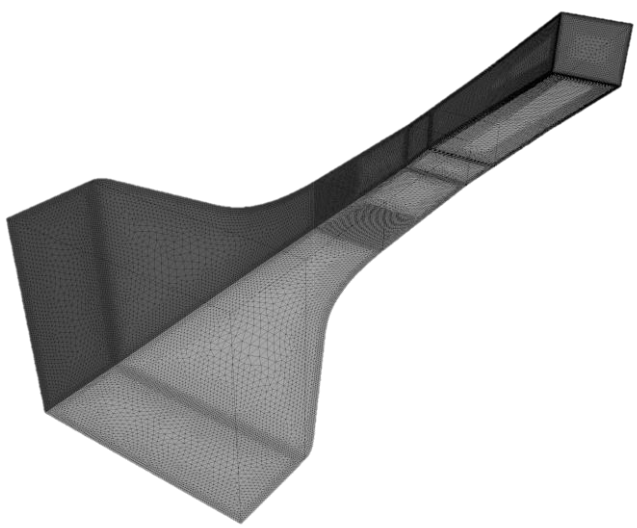

Figure 3 Surface grid

D. Boundary Conditions (BC)

The selection and application of the appropriate boundary conditions was an integral part of the study. At the entrance to the settling chamber, a jet boundary condition available in USM3D flow solver was applied. The jet boundary condition was set by defining the total pressure and total temperature at the entrance plane. These values were obtained from the tunnel data acquisition system for the appropriate test condition.

Two different boundary conditions at the exit of the first diffuser were evaluated and each had their own advantages and disadvantages. The procedures used to set the tunnel speed in the test section depended on the exit BC that was used.

3. Extrapolation Boundary Condition

The extrapolation BC extrapolates the density, velocities and pressures from an interior domain cell to the outflow boundary using a Taylor series expansion. To set the desired test section conditions, the freestream Mach number M_∞ in the solver was iterated until the desired target Mach number was reach at tunnel station 17.75.

4. Internal Outflow Boundary Condition

The internal outflow BC extrapolates density and velocities, and sets the static pressure to a constant freestream value on the outflow boundary. Total enthalpy is also imposed at the exit boundary. To set the desired test section conditions, M_∞ in the input was set to the desired Mach number in the test section, and the static pressure at the exit of the diffuser was iterated until the desired target Mach number was reached at tunnel station 17.75. The internal outflow BC has the advantage that the input M_∞ is the proper value that would be used to non-dimensionalize the forces and moments if an aircraft configuration was modeled in the test section.

IV. Results

The data will be presented by comparing the results obtained using the two different exit boundary conditions, followed by a comparison between the two different geometry sources. In all cases, the test conditions that were evaluated were at a target Mach number of 0.2678 and a Reynolds number of 1.71×10^6/ft.

A. Boundary condition comparison

The Mach contours for the plane z = 0.0 in the high-speed leg are shown in Figure 4. It shows a smooth acceleration of the flow to the target Mach number in the test section followed by the deceleration in the 1st diffuser. Figure 4b does show what is thought to be an interaction of the flow with the boundary at the very exit of the diffuser, and is still under investigation. Figure 5 shows a profile of the Mach number at reference station 17.75. The processes used to set the target Mach number in the test section were successful and both boundary conditions provided very similar profiles

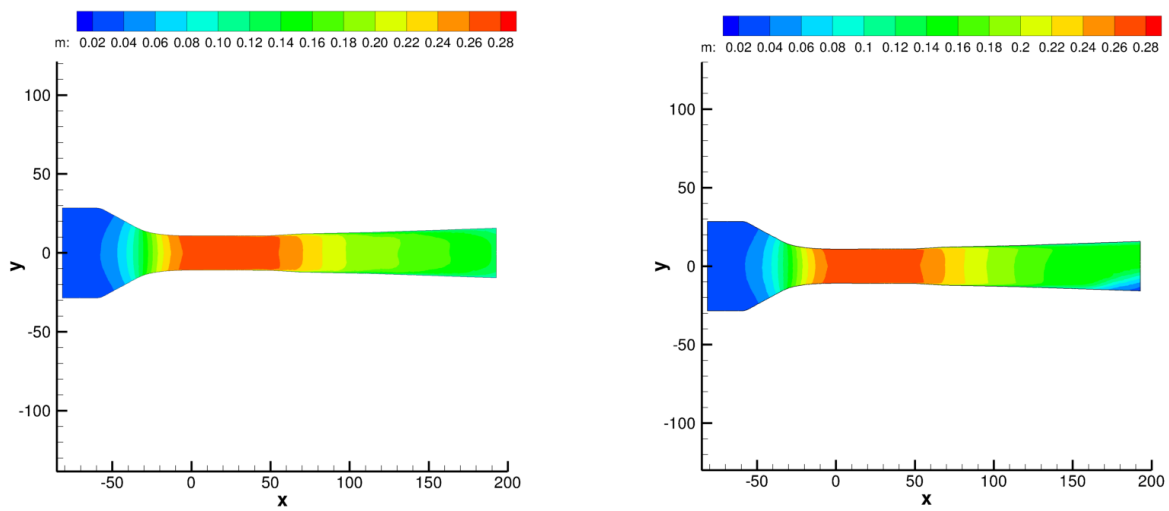

(a) Extrapolation BC (b) Internal Outflow BC

Figure 4 Mach contours, z = 0 plane

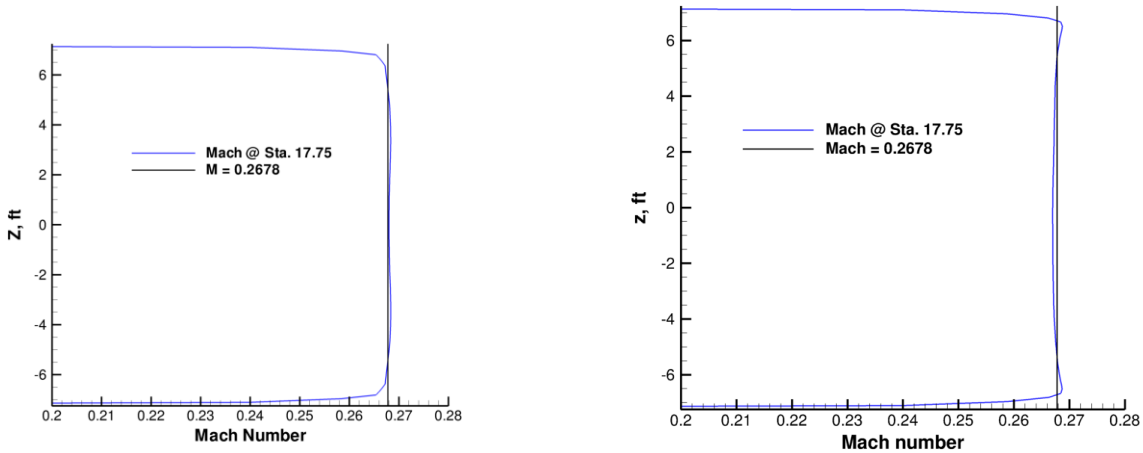

(a) Extrapolation BC (b) Internal Outflow BC

Figure 5 Mach profile, y = 0.0

The boundary layer is allowed to grow naturally all the way from the settling chamber and to the exit of the diffuser. Figure 6 shows a comparison between the measured and predicted boundary layer at Station 7.87. It is presented using the non-dimensional y^+ and u^+ coordinates to evaluate how well the structure of the turbulent boundary layer is captured. The experimental data was obtained by taking the measured velocity from a boundary layer probe in the test section and transforming to non-dimensional units by the Clauser[10] method and then fitting the data to Spalding's curve. The numerical results pick up the buffer region very well and match the slope of the log-law portion of the boundary layer. The wake region of the boundary layer is well represented, but there is a difference between the results from the two boundary conditions that is still be investigated.

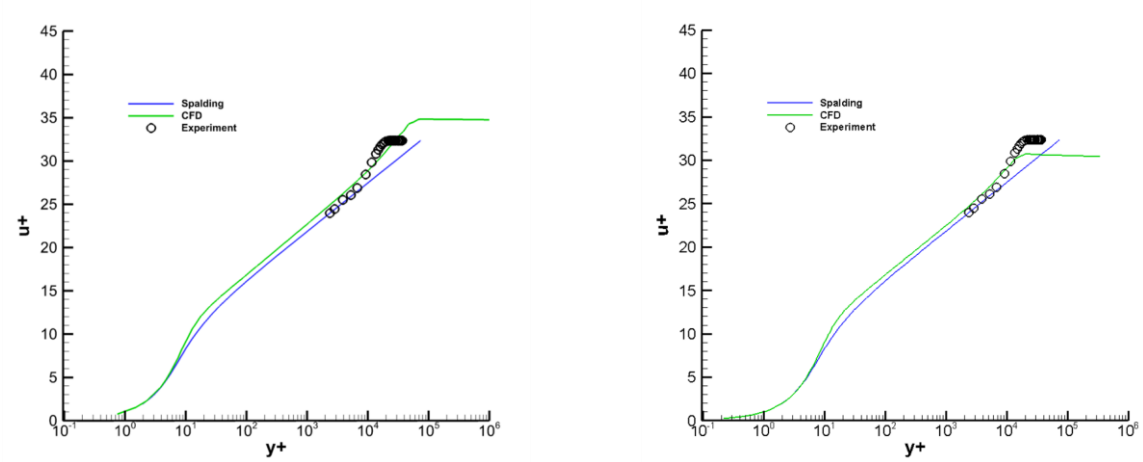

(a) Extrapolation BC (b) Internal Outflow BC

Figure 6 Boundary layer profile, y = 0.0, Sta. = 7.87

Flow angularity can detect small changes in the flow field and present a picture of the flow uniformity in the test section. Figure 7 shows a comparison of the predicted upwash angle with the two different exit BCs, at several stations throughout the test section for the case of geometry developed from construction drawings. In either case the effects of the straight 90 deg wall corners in the contraction and test section are clearly visible. Both cases show these effects to dissipate.

Flow angularity is a commonly used parameter for correcting experimental data in the tunnel. Experimentally the upwash angle is determined by conducting an alpha sweep with a model in the tunnel in both an upright and inverted configuration. Half the distance between the two lift curves provides a measure of an integrated (over the span of the wing) upwash angle. Reference 5 states that at the time of publication, the indicated upwash angle was approximately 0.15 degree. Figure 7(c) and (d) show the predicted upwash at station 17.75, which is where the

check standard model is located. Looking at the z=0 data the predicted upwash angle is on the order of 0.05 degrees.

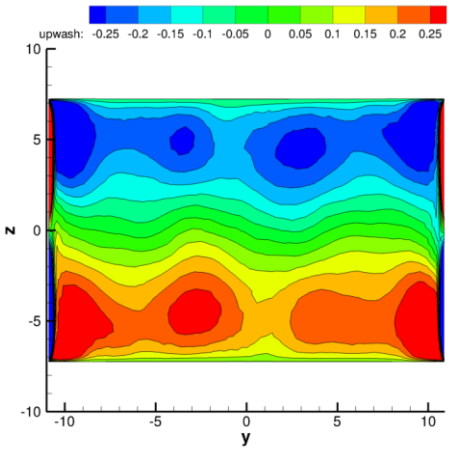

(a) Extrapolation BC, Sta. 0.0

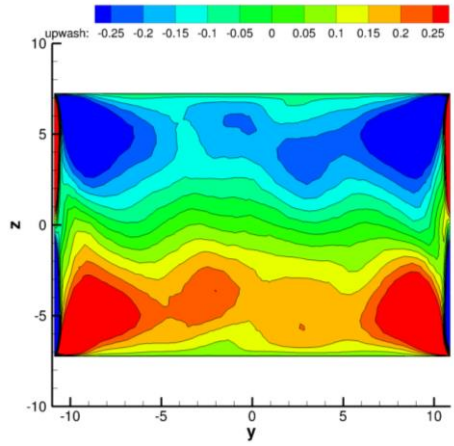

(b) Internal Outflow BC, Sta. 0.0

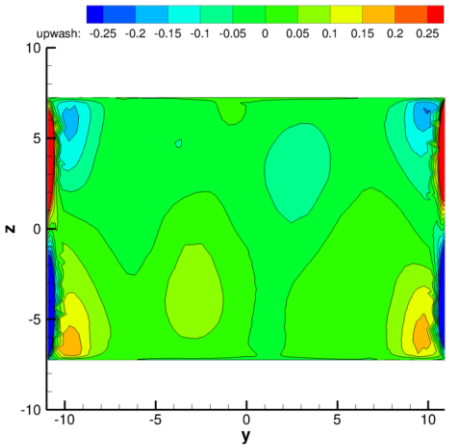

(c) Extrapolation BC, Sta. 17.75

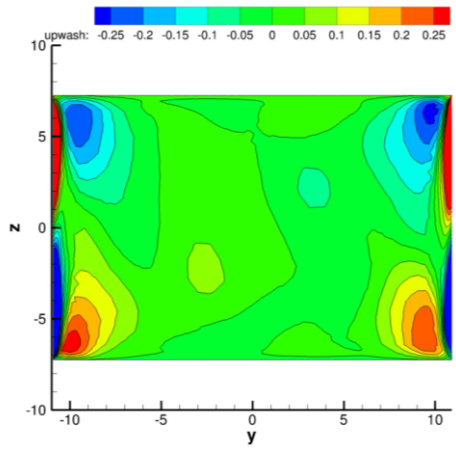

(d) Internal Outflow BC, Sta. 17.75

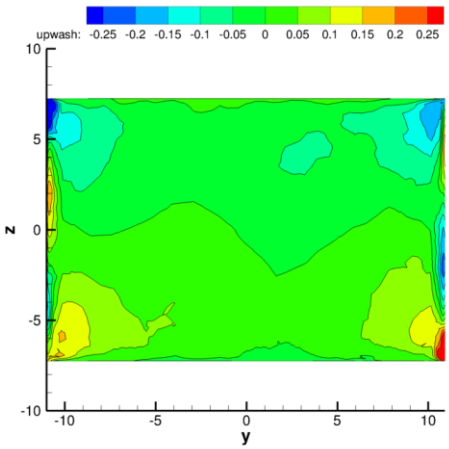

(e) Extrapolation BC, Sta. 50.

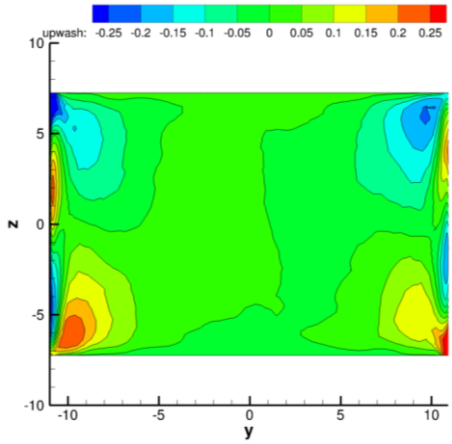

(f) Internal Outflow BC, Sta. 50.

Figure 7 Contours of upwash angle (geometry from construction drawings)

B. Geometry comparison

The data presented in this section will compare the effects of using the construction drawings "as designed" or the laser-scanned "as built" surfaces. All the data will be shown using the internal outflow BC described above. The Mach contours for the plane z = 0.0 in the high-speed leg are shown in Figure 8. There is a slight difference in the settling chamber and the entrance to the contraction due to the fairing over the screen and honeycomb supports. There is also a small difference in the region of the 1st diffuser air intake (sta. 115) that is due to slightly different ways of fairing over the vents. The small region of reduced Mach number at the exit boundary are still present for the internal outflow BC, but the region has switch to the upper edge with the scanned surfaces. This issue will further be investigated by comparing results from another unstructured grid code.

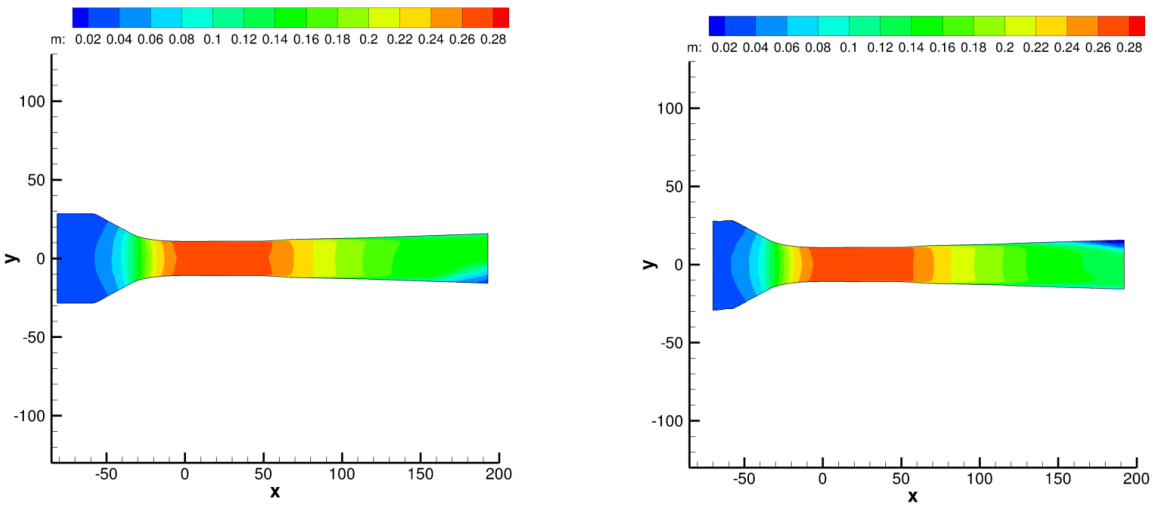

(a) Construction drawings (b) Scanned surfaces

Figure 8 Mach contours, z= 0 plane

Figure 9 shows the Mach number profile at station 17.75 for both sets of geometries. Both geometry definitions provide a uniform profile. Figure 10 shows a comparison of the boundary layer profiles based on the two sets of geometries. In either case, a nearly identical profile is obtained.

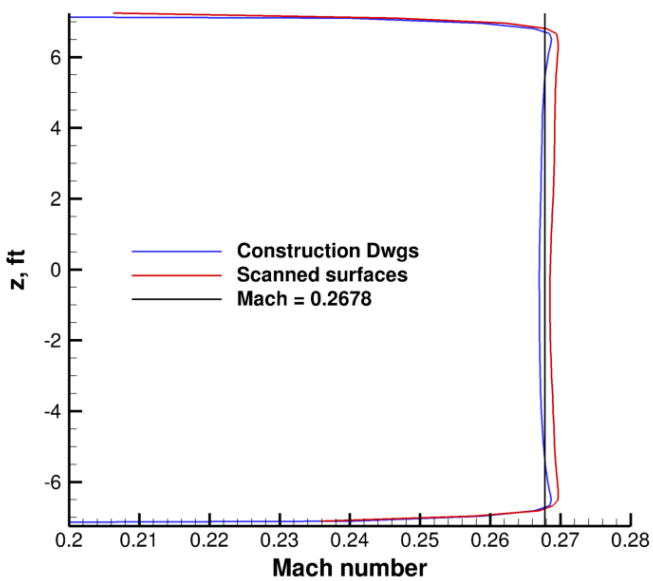

Figure 9 Mach profile, y = 0.0, Sta. = 17.75

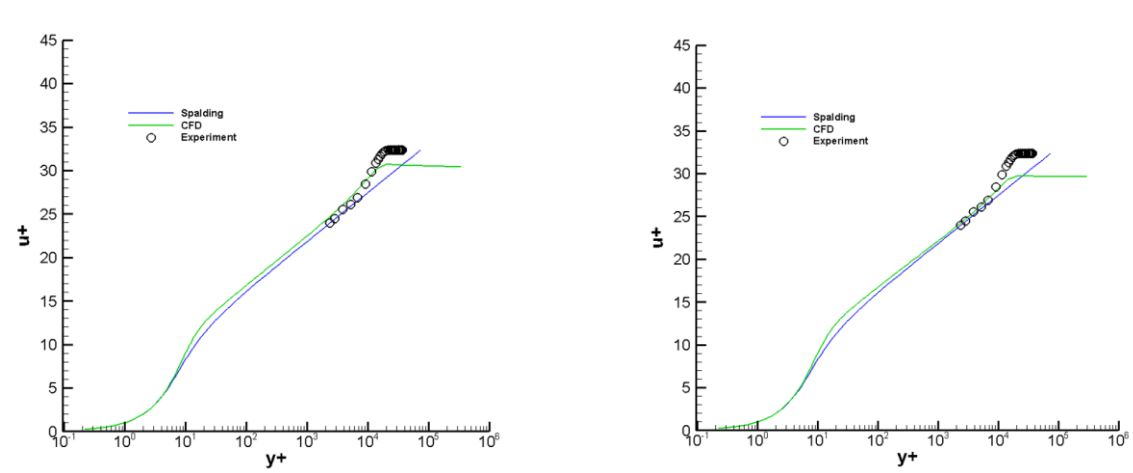

(a) Construction drawings (b) Scanned surfaces

Figure 10 Boundary layer profile, y = 0.0, Sta. = 7.87

Figure 11 shows a comparison of the predicted upwash angles with the two geometry definitions. One can now see a substantial difference between the two predictions. As before, the upwash angles based on the construction drawings (as designed) show the corner disturbances being generally symmetrical and decaying toward the end of the test section. The upwash angles based on the scanned surfaces (as built) show much stronger and asymmetrical disturbances near the tunnel floor An investigation is underway to determine what are the differences between these two geometry definitions. Comparing the upwash angles at z = 0.0 in Figure 11(c) and (d) the upwash angles for the scanned surfaces are now approaching 0.1 deg, which is closer to that measured with the check standard model.

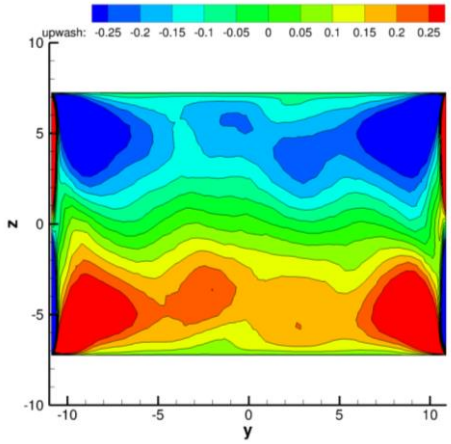

(a) Construction Drawings, Sta. 0.0

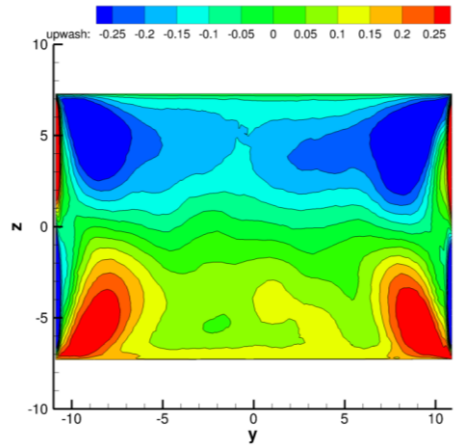

(b) Scanned Surfaces, Sta. 0.0

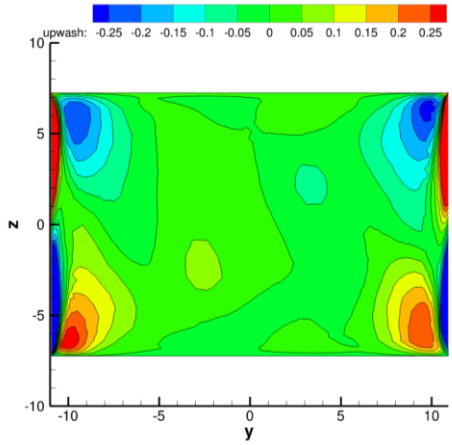

(c) Construction Drawings, Sta. 17.75

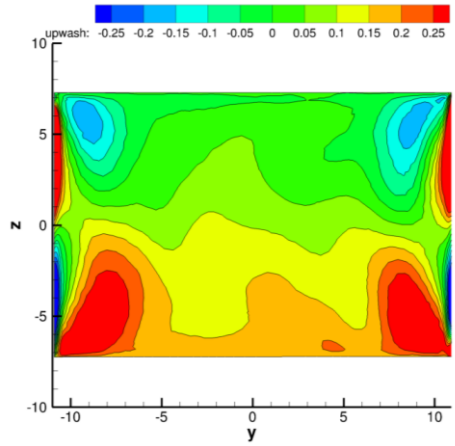

(d) Scanned Surfaces, Sta. 17.75

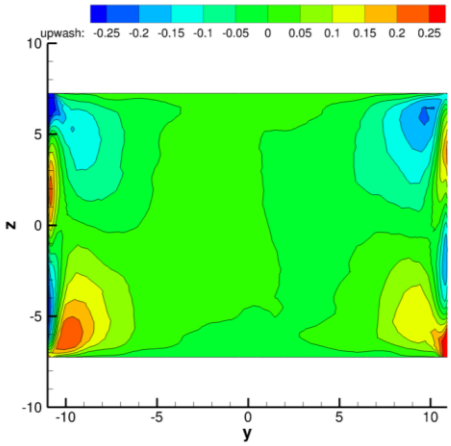

(e) Construction Drawings, Sta. 50.

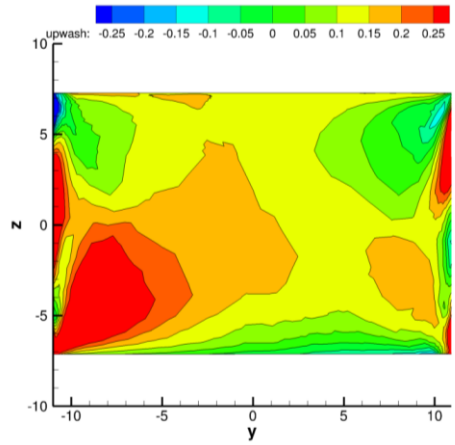

(f) Scanned Surfaces, Sta. 50.

Figure 11 Contours of upwash angle

Figure 12 shows the static pressure along the centerline of the tunnel. The computational results are compared with the experimental data from Reference 5. The experimental results were obtained through the use of a centerline probe, which spanned the distance from 20 ft into the contraction to the end of the test section. The experimental data show that the static pressure decreases 0.0959 psf/ft from Sta. 5 to Sta. 30. A further decrease in static pressure

occurs between Sta. 30 to 40 as the free stream flow adjusts to the 3-ft slot opening in the tunnel walls. Those slots are not modeled in the paper as they have been permanently closed. Future work will include modeling the centerline probe and supporting structure.

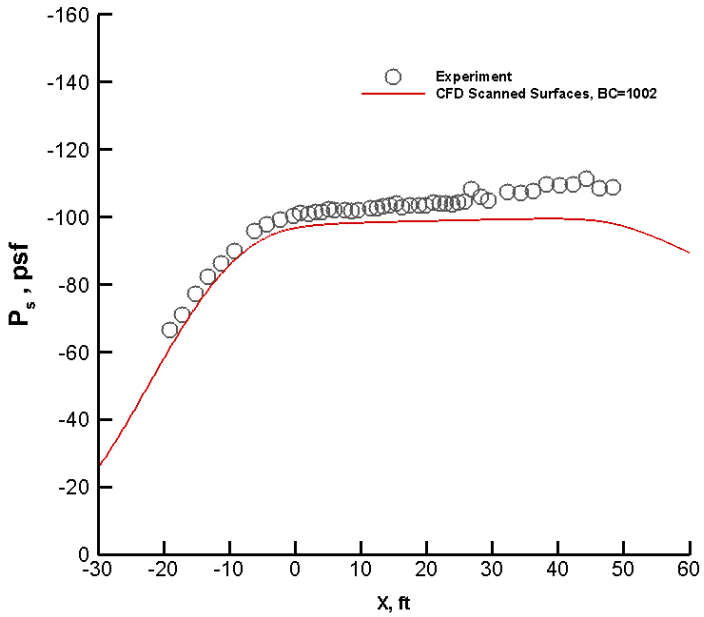

Figure 12 Centerline pressures

V. Concluding Remarks

Numerical simulations of the high-speed leg of the 14 x 22-ft wind tunnel have been presented. Results from two different diffuser exit boundary conditions and two different geometry standards are shown. The two geometry standards represent an "as designed" and an "as built" comparison. The two exit boundary conditions have shown to provide very similar results with the exception of an interaction at the exit boundary with the internal outflow boundary conditions. The two geometry standards show generally overall agreement, but the upwash angles in the test section show a strong asymmetry in the corners near the floor that are being further investigated.

Acknowledgments

Funding for this work has been provided by Research Directorate of NASA Langley Research Center under LASER0175 contract. The authors would like to thank William Ball of NASA Langley and Jason Hall of Stinger Ghaffarian Technologies (SGT) for their efforts in providing the laser-scanned point-cloud data for this investigation.

References

[1] Rogers, Stuart, E. and Roth, Karlin: "CFD Validation of High-Lift Flows With Significant Wind-Tunnel Effects" AIAA Paper 2000-4218, 18th AIAA Applied Aerodynamics Conference, 14-17, Denver, CO, August 2000

[2] Olander, Mattias: "CFD Simulation of the Volvo Cars Slotted Wind Tunnel", *Masters Thesis* 2011:33, Chalmers University of Technology, Dept. of Applied Mechanics, 2011

[3] Wall, Anette: "Simulating the Volvo Cars Aerodynamic Wind Tunnel with CFD", *Masters Thesis* 2013:08, Chalmers University of Technology, Dept. of Applied Mechanics, 2013

[4] Rumsey, C., Slotnick, J., Long, M., Stuever, R., Wayman, T., "Summary of the First AIAA CFD High Lift Prediction Workshop," AIAA-2011-939, Jan 2011.

[5] Gentry, Garl L., Jr., Quinto, P. Frank, Applin, Zachary T.: "The Langley 14- by 22-Foot Subsonic Tunnel: Description, Flow Characteristics, and Guide for Users" NASA TP-3008, September, 1990.

[6] Frink, N. T., Pirzadeh, S. Z., Parikh, P. C., Pandya, M. J., and Bhat, M.K.: "The NASA Tetrahedral Unstructured Software System," *The Aeronautical Journal*, Vol. 104, No. 1040, October 2000, pp. 491-499

[7] Samareh, J. A.: "GridTool: A Surface Modeling and Grid Generation Tool", *Proceedings of the Workshop on Surface Modeling, Grid Generation, and Related Issues in CFD Solutions*, NASA Lewis Research Center, Cleveland, OH, NASA CP-3291, 1995, May 9-11, 1995

[8] Lohner, R. and Parikh, P., "Three-Dimensional Grid Generation By The Advancing Front Method," *International Journal for Numerical Methods in Fluids*," Vol. 8, Issue 10, 1988, pp. 1135-1149

[9] Pirzadeh, S. Z.: "Three Dimensional Unstructured Grids By The Advancing Layer Method," *AIAA Journal*, Vol. 33, No. 1, 1996, pp. 43-49

[10] Clauser, Francis H.: "Turbulent Boundary Layers in Adverse Pressure Gradients", *Journal of the Aeronautical Sciences*, Vol. 21, No. 2, 1954, pp. 91-108.